

The total infrared luminosity may significantly overestimate the star formation rate of quenching and recently quenched galaxies

Christopher C. Hayward^{1,2*}†, Lauranne Lanz³, Matthew L. N. Ashby⁴, Giovanni Fazio⁴, Lars Hernquist⁴, Juan Rafael Martínez-Galarza⁴, Kai Noeske⁵, Howard A. Smith⁴, Stijn Wuyts⁶ and Andreas Zezas^{4,7,8}

¹TAPIR, Mailcode 350-17, California Institute of Technology, 1200 E. California Boulevard, Pasadena, CA 91125, USA

²Heidelberger Institut für Theoretische Studien, Schloss–Wolfsbrunnenweg 35, 69118 Heidelberg, Germany

³Infrared Processing and Analysis Center, California Institute of Technology, 1200 E. California Boulevard, Pasadena, CA 91125, USA

⁴Harvard–Smithsonian Center for Astrophysics, 60 Garden Street, Cambridge, MA 02138, USA

⁵Space Telescope Science Institute, 3700 San Martin Drive, Baltimore, MD 21218, USA

⁶Max-Planck-Institut für extraterrestrische Physik, Postfach 1312, Giessenbachstrasse 1, 85741 Garching, Germany

⁷University of Crete, Physics Department & Institute of Theoretical & Computational Physics, 71003 Heraklion, Crete, Greece

⁸Foundation for Research and Technology–Hellas, 71110 Heraklion, Crete, Greece

Submitted to MNRAS

ABSTRACT

The total infrared (IR) luminosity is very useful for estimating the star formation rate (SFR) of galaxies, but converting the IR luminosity into an SFR relies on assumptions that do not hold for all galaxies. We test the effectiveness of the IR luminosity as an SFR indicator by applying it to synthetic spectral energy distributions generated from three-dimensional hydrodynamical simulations of isolated disc galaxies and galaxy mergers. In general, the SFR inferred from the IR luminosity agrees well with the true instantaneous SFR of the simulated galaxies. However, for the major mergers in which a strong starburst is induced, the SFR inferred from the IR luminosity can overestimate the instantaneous SFR during the post-starburst phase by greater than two orders of magnitude. Even though the instantaneous SFR decreases rapidly after the starburst, the stars that were formed in the starburst can remain dust-obscured and thus produce significant IR luminosity. Consequently, use of the IR luminosity as an SFR indicator may cause one to conclude that post-starburst galaxies are still star-forming, whereas in reality, star formation was recently quenched.

Key words: dust, extinction – galaxies: interactions – galaxies: starburst – infrared: galaxies – radiative transfer – stars: formation.

1 INTRODUCTION

The total infrared (IR) luminosity (L_{IR}) of galaxies has been used to infer the star formation rate (SFR) of galaxies for decades (see Kennicutt 1998b and Kennicutt & Evans 2012 for reviews). Since the launch of the *Herschel Space Observatory*, the IR luminosity has been often used to infer the SFRs of diverse types of local and high-redshift galaxies (e.g. Rodighiero et al. 2010; Elbaz et al. 2011; Wuyts et al. 2011a; Magnelli et al. 2012; Rosario et al. 2012, 2013; Lee et al. 2013).

Using the IR luminosity as an SFR indicator has several advantages. For example, other SFR indicators, such as recombination lines (e.g. $\text{H}\alpha$) and ultraviolet (UV) emission, must be corrected for dust attenuation to recover the intrinsic SFR. Correcting

for dust is inherently uncertain because the observed emission is dominated by the less-obscured lines of sight; consequently, the dust attenuation can be underestimated. In contrast, the IR is a promising SFR indicator precisely because of dust: in the limit of high obscuration, essentially all of the UV-optical light from young stars is absorbed and re-emitted into the IR. Thus, the IR luminosity should be the best SFR indicator in those situations, such as for starburst galaxies. Furthermore, the IR luminosity can be combined with tracers of unobscured star formation (uncorrected for dust attenuation); such combinations may yield more accurate SFR estimates (e.g. Kennicutt et al. 2007; Kennicutt et al. 2009; Relaño & Kennicutt 2009; Wuyts et al. 2011a,b; Reddy et al. 2012; Lanz et al. 2013).

Naturally, there are also caveats to using the IR luminosity as an SFR indicator because multiple assumptions must be made to convert the IR luminosity into an SFR (see Kennicutt 1998b for a more thorough discussion). As with all SFR indicators, the

* E-mail: christopher.hayward@h-its.org

† Moore Prize Postdoctoral Scholar in Theoretical Astrophysics

IR luminosity is sensitive to the initial mass function (IMF; e.g. Narayanan & Davé 2012). The sensitivity to the high end of the IMF is less severe for the IR than for recombination lines because the IR light originates from dust that is heated by both lower-mass stars and the massive stars that photoionise nebulae and thereby generate recombination line emission. However, this effect can also be a disadvantage of using the IR luminosity as an SFR indicator: it is commonly stated (e.g. Kennicutt 1998b) that, similar to the UV, the IR luminosity is sensitive to the SFR averaged over the past ~ 100 Myr (in contrast, recombination lines are sensitive to the SFR averaged over the past ~ 10 Myr). Thus, the IR luminosity may not trace the instantaneous SFR accurately if it varies over timescales of $\lesssim 100$ Myr.

Furthermore, dust can also be heated by older stars; if such dust heating is non-negligible, as has been suggested by some authors (e.g. Sauvage & Thuan 1992; Smith et al. 1994; Smith & Harvey 1996; Walterbos & Greenawalt 1996; Kennicutt et al. 2009; Salim et al. 2009; Calzetti et al. 2010; Kelson & Holden 2010; Murphy et al. 2011; Totani et al. 2011; Groves et al. 2012; Leroy et al. 2012; Fumagalli et al. 2013; Utomo et al. 2014) converting the IR luminosity into an SFR using a standard calibration will overestimate the true SFR. This effect becomes increasingly important with decreasing SFR (Calzetti et al. 2010; Smith et al. 2012; Rowlands et al. 2014; Utomo et al. 2014). When the contribution of older stellar populations to dust heating is non-negligible, the implicit averaging timescale is $\gg 100$ Myr (Salim et al. 2009; Kelson & Holden 2010). Emission from active galactic nuclei (AGN) can also heat dust and thus cause the IR-inferred SFR to overestimate the true SFR. The IR-inferred SFR can also under-predict the true SFR if a significant fraction of the photons from young stars is not absorbed by dust or if stellar populations younger than 100 Myr dominate the bolometric luminosity (e.g. Schaerer et al. 2013; Sklias et al. 2014).

In this paper, we quantify the effectiveness of the IR luminosity as an SFR indicator by applying it to mock spectral energy distributions (SEDs) calculated from three-dimensional hydrodynamical simulations of isolated disc galaxies and galaxy mergers. Because the simulated galaxies have star formation histories that are significantly more complex than those assumed to calibrate the L_{IR} -SFR relation (i.e., a single burst or continuous star formation history), realistically treat dust attenuation from both stellar birth clouds and the diffuse interstellar medium (ISM), and include AGN emission, they can be used to characterise the effects of some of the aforementioned assumptions that may cause the IR luminosity to poorly trace the instantaneous SFR. The remainder of this work is organised as follows: in Section 2, we briefly summarise the details of the simulations. In Section 3, we compare the L_{IR} -inferred SFR and true instantaneous SFR and the resulting inferred and true SFR–stellar mass (M_*) relations. In Section 4, we discuss some implications of our results and ways forward.

2 METHODS

The simulations used in this work are a subset of those used in Lanz et al. (2014, hereafter L14). We briefly describe them here, but we refer the reader to that work for full details. We performed three-dimensional hydrodynamical simulations of four isolated disc galaxies and binary mergers of all possible combinations of those galaxies for a single (non-special) orbit (thereby yielding ten merger simulations) using the N -body/smoothed-particle

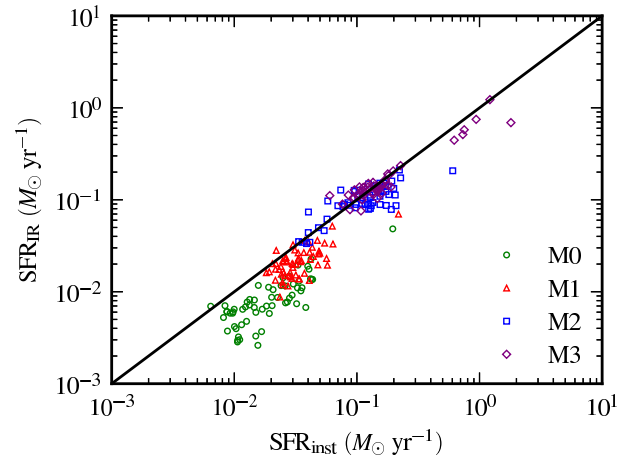


Figure 1. SFR inferred from the IR luminosity vs. the instantaneous SFR for simulated isolated disc galaxies. The points are coloured according to the simulation from which they originate. The black line indicates equality. The inferred and actual SFR typically agree well. For the lower-mass galaxies, a significant fraction of the photons emitted by young stars is not absorbed; consequently, the SFR is slightly underestimated.

hydrodynamics (SPH) code GADGET-3 (Springel 2005).¹ The progenitor disc galaxies are referred to as M0, M1, M2, and M3, where a higher number indicates a greater mass; the masses of the stellar discs of (M0, M1, M2, M3) are $(0.061, 0.38, 1.18, 4.22) \times 10^{10} M_{\odot}$, and other galaxy properties, such as the gas fraction and disc scale length, are varied such that the galaxies represent typical local galaxies (Jonsson et al. 2006; Cox et al. 2008). The major (equal-mass) merger simulations used in this work are referred to as M0M0e, M1M1e, M2M2e, and M3M3e, which correspond to mergers of two M0, M1, M2, and M3 disc galaxies, respectively, on the e orbit of Cox et al. (2006).

The simulations include gas cooling and simple models for star formation, the multiphase ISM (Springel & Hernquist 2003), and black hole accretion and AGN feedback (Springel et al. 2005b). The star formation rate of the simulations is calculated on a particle-by-particle basis: each gas particle with density greater than a threshold density ($n_{\text{H}} \sim 0.1 \text{ cm}^{-3}$) is assigned an SFR according to a volume-density-dependent Kennicutt–Schmidt prescription (Schmidt 1959; Kennicutt 1998a), $\rho_{\text{SFR}} \propto \rho^N$; we assume $N = 1.5$. Summing the SFRs of the individual gas particles yields the total instantaneous SFR of the galaxy, SFR_{inst} . In practice, star formation is implemented by stochastically converting gas particles into star particles, where the probability of a gas particle being converted into a star particle depends on its SFR.

To calculate mock SEDs of the simulated galaxies, we perform three-dimensional dust radiative transfer in post-processing at multiple times throughout each GADGET-3 simulation using the Monte Carlo dust radiative transfer code SUNRISE (Jonsson 2006; Jonsson, Groves, & Cox 2010). The star and black hole particles in the GADGET-3 simulations are the sources of radiation, and

¹ Recently, various authors have highlighted issues with the standard formulation of SPH that may cause the results of simulations performed using the technique to be inaccurate. However, for the type of idealised simulations used in this work, the standard form of SPH yields results that are very similar to those of the more-accurate moving-mesh hydrodynamics technique (Hayward et al. 2014).

the metal distribution determines the dust distribution; we assume that 40 per cent of the metals are in dust (e.g. James et al. 2002; Sparre et al. 2014a). We use the default ISM model of L14, which is a conservative choice because it exhibits less dust attenuation than the alternative model, and we have checked that our conclusions are insensitive to whether we use the default or alternative ISM treatments. Given these inputs, radiative transfer is performed to calculate the absorption, scattering, and re-emission of stellar and AGN light by dust.

These or similar simulations have been demonstrated to provide good matches to the SEDs of local disc galaxies (Jonsson et al. 2010), local interacting galaxies (L14), and high-redshift obscured starbursts and AGN (Narayanan et al. 2009, 2010a,b; Snyder et al. 2013; E. Roebuck et al., in preparation). Furthermore, at different times in their evolution, they reproduce various properties of other populations, including submillimetre galaxies (e.g. Hayward et al. 2011, 2012, 2013), post-starburst galaxies (Snyder et al. 2011), and compact quiescent galaxies (Wuyts et al. 2010), among others. The success of the models supports our use of them to test how well L_{IR} traces the instantaneous SFR.

3 RESULTS

To infer the SFR from the IR luminosity of our simulated galaxies, we first integrate the (spatially integrated) galaxy SEDs over the wavelength range 8 – 1000 μm to calculate L_{IR} . We adopt this wavelength range following Kennicutt (1998b), but the precise definition (e.g. if we use only the far-IR, FIR) is unimportant for our conclusions because the FIR luminosity dominates L_{IR} . Then, we convert L_{IR} to an SFR using the following relation:

$$\text{SFR}_{\text{IR}} = 3.0 \times 10^{-37} \left(\frac{L_{\text{IR}}}{\text{W}} \right) M_{\odot} \text{ yr}^{-1}, \quad (1)$$

which is the Kennicutt (1998b) conversion factor converted to the Kroupa (2001) IMF by dividing by 1.5 (e.g. Schiminovich et al. 2007). We have made this conversion because the Kroupa IMF is assumed when calculating the STARBURST99 (Leitherer et al. 1999) single-age stellar population SEDs that are used as input for the radiative transfer calculations; thus, we must use the same IMF for the calibration for consistency. Also, we note that this factor is calculated by assuming continuous bursts of age 10–100 Myr, and Kennicutt (1998b) explicitly states that strictly speaking, it is valid only for starbursts that are less than 100 Myr old. Nevertheless, this conversion is routinely applied to diverse galaxy types, including those for which detailed information about their SFHs is unavailable (e.g. for high-redshift galaxies).

3.1 Isolated disc galaxies

Fig. 1 compares the SFR inferred from the IR luminosity using Equation (1) and the instantaneous SFR² for simulated isolated

² The ‘instantaneous SFR’ of the simulated galaxies is the sum of the SFRs of the individual gas particles, which are calculated based on their gas densities and the assumed sub-resolution star formation prescription. Consequently, the instantaneous SFR value for the simulations corresponds to an average over a timescale that is less than the maximum time step, 5 Myr. The exact timescale is not well-defined because adaptive time steps are used. However, the salient feature of the SFR value of the simulations is that the averaging timescale is less than that of any of the observable SFR tracers.

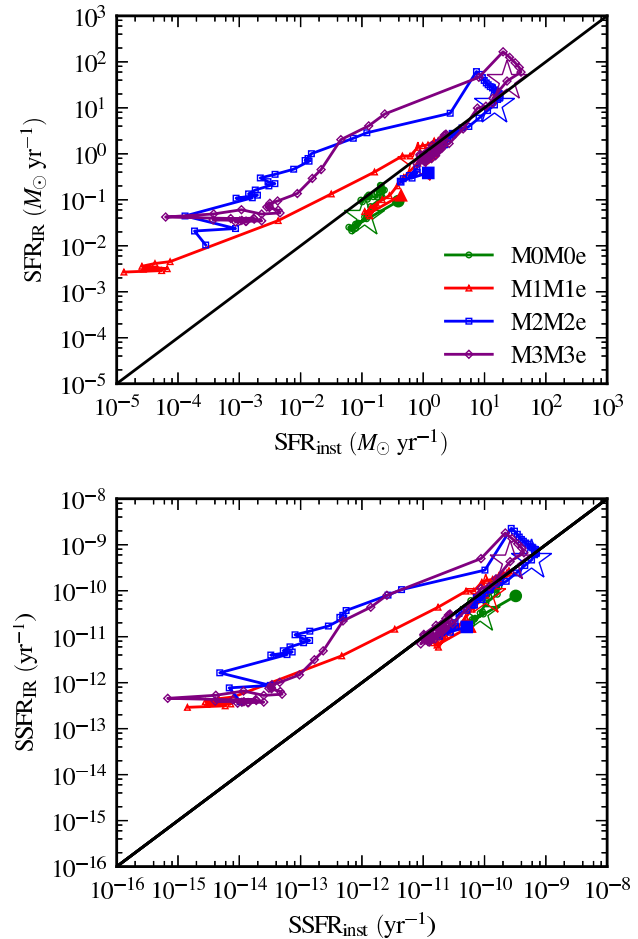


Figure 2. SFR (top) and SSFR (bottom) inferred from the IR luminosity vs. the instantaneous SFR (SSFR) for the major merger simulations. The data points are connected to illustrate the time evolution. Near coalescence of the black holes, which is indicated by a star, the data points are separated by 10 Myr. At other times, the separation is 100 Myr. The large filled symbols indicate the start of each simulation. In the simulations in which a strong starburst is induced, the IR-inferred SFR (SSFR) can overestimate the instantaneous SFR (SSFR) in the post-starburst phase by greater than two orders of magnitude. Note that for fixed SSFR (of $\gtrsim 10^{-11} \text{ yr}^{-1}$), the overestimation occurs only in the post-starburst phase of the simulations. This indicates that the time evolution of the SSFR, not just the value of the instantaneous SSFR, determines whether the IR luminosity overestimates the SSFR.

disc galaxies. The data are coloured according to the simulation from which they originate. For the major mergers, the data points are connected to illustrate the time evolution. The start of each simulation is marked with a larger filled symbol, and the time of coalescence of the central black holes is marked with a star. In this and the following figures, we show the results for a single viewing angle because the SFR is independent of viewing angle by definition, and the variation in L_{IR} with viewing angle is $\lesssim 10$ percent (we note that the variation with viewing angle can be more significant in high-redshift, gas-rich mergers; Hayward et al. 2012).

The inferred and true SFRs agree well for the isolated discs, although the IR luminosity tends to underestimate the SFR of the least-massive disc galaxy (M0). The reason for the underestimation is that this galaxy is not sufficiently dust-obscured. Thus, a

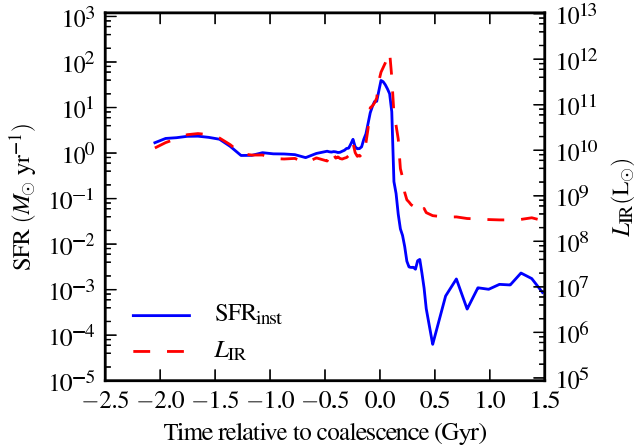


Figure 3. SFR (solid blue line) and L_{IR} (dashed red line) vs. time relative to coalescence for the most-massive major merger simulation (M3M3e). The values on the left (SFR) and right (L_{IR}) axes are related through Eq. (1); thus, the IR-inferred SFR can be read off from the L_{IR} curve by referring to the left axis. Until the peak of the starburst, L_{IR} has a similar evolution to the SFR, and thus the IR-inferred SFR agrees with the true SFR. However, after the starburst, L_{IR} decreases much more gradually than the SFR because there is significant dust heating from stars that formed during the burst; thus, L_{IR} is a poor tracer of the SFR in this regime.

significant fraction of the light from young stars escapes the galaxy without being absorbed by dust.

3.2 Galaxy mergers

Fig. 2 compares the IR-inferred and true instantaneous SFR (top) and specific SFR ($\text{SSFR} \equiv \text{SFR}/M_*$; bottom) values for the major merger simulations. The inferred and actual (S)SFR values agree very well for much of the mergers’ evolution. However, there is an important exception: in the simulations in which a strong starburst is induced near coalescence (all but M0M0e), the IR-inferred (S)SFR significantly overestimates the instantaneous (S)SFR in the post-starburst phase. This overestimation first occurs immediately after the maximum SFR of the starburst is attained, and it can persist for hundreds of Myr (until the end of the simulations). At the lowest (S)SFRs, the instantaneous (S)SFR can be overestimated by greater than two orders of magnitude.

One might expect that the SSFR determines whether older stellar populations contribute significantly to the IR luminosity: for actively star-forming galaxies (i.e. those with high SSFR values), young stars should dominate the dust heating, whereas for galaxies with low SSFR values, dust heating from older stellar populations may be significant. Indeed, the bottom panel of Fig. 2 indicates that the overestimation is more significant for lower SSFR values. However, this panel also indicates that the instantaneous value of the SSFR is not the sole determinant of how well the IR luminosity can be used to recover the (S)SFR: for fixed SSFR (of $\gtrsim 10^{-11} \text{ yr}^{-1}$, which is the minimum SSFR value during the pre-starburst phase of the simulations), the overestimation occurs only during the post-starburst phase of the simulations. Thus, the time evolution of the SSFR, not just the instantaneous value, is important for determining how well the IR luminosity traces the (S)SFR.

To clarify the reason for the overestimation, we show the time evolution of the SFR and L_{IR} for one of the major merger simulations, M3M3e (the most-massive simulation in our suite), in Fig.

3. Near the time of final coalescence of the two galaxies, a strong starburst is induced because tidal forces drive gas into the nuclear region and consequently, the gas density and thus SFR increase sharply. In the starburst, the instantaneous SFR increases by a factor of ~ 30 in < 200 Myr. Subsequently, because most of the gas has been consumed by star formation or heated by shocks and AGN feedback (i.e., the star formation is ‘quenched’), the SFR plummets by greater than four orders of magnitude. Afterward, the SFR remains very low, and the galaxy is a passively evolving spheroid.

Until the peak of the starburst, the evolution of the SFR and L_{IR} is essentially identical. However, after the peak of the starburst, when the SFR decreases very rapidly, this similarity no longer holds. Rather, L_{IR} declines more gradually; this difference is the origin of the aforementioned discrepancy between the SFR inferred from L_{IR} and the instantaneous SFR. Part of the reason for the difference is that during the starburst, the SFR varies significantly on timescales of less than 100 Myr. Consequently, the instantaneous SFR and SFR averaged over the past 100 Myr differ significantly at this time. Thus, one of the fundamental assumptions of the L_{IR} -SFR conversion does not hold. However, the overestimation persists and actually becomes more severe well after the starburst, when the instantaneous SFR is relatively constant on a 100-Myr timescale.

The fundamental reason for the overestimation is that although the SFR is extremely low ($\sim 10^{-3} M_{\odot} \text{ yr}^{-1}$) after the starburst, a significant number of young stars (with ages of 100s of Myr) remain. These stars are still very luminous and obscured and hence can effectively heat the dust and thus yield significant IR emission. Consequently, the effective averaging timescale for the IR-inferred SFR is $\gg 100$ Myr during the post-starburst phase of the simulations.

In principle, the AGN can also heat the dust and result in IR emission. By re-running the radiative transfer calculations with the AGN disabled, we have confirmed that dust heated by AGN is not the dominant cause of the overestimation (in all but a few snapshots of these simulations, L_{IR} decreases by $\lesssim 50$ per cent when the AGN emission is disabled). Nevertheless, FIR emission from AGN-heated dust can be important in some regimes and will be a subject of future work (L. Rosenthal et al., in preparation).

3.3 Implications for the SFR-stellar mass relation

The overestimation demonstrated above has significant consequences for interpreting IR observations (from e.g. *Herschel* and the Atacama Large Millimeter/submillimeter Array, ALMA) of galaxies that have recently undergone strong starbursts. One topic for which this overestimation is potentially significant is the SFR- M_* relation (aka ‘main sequence’) of star-forming galaxies (Brinchmann et al. 2004; Salim et al. 2005; Noeske et al. 2007; Daddi et al. 2007). Fig. 4 shows SFR vs. M_* for the major merger simulations for both the true instantaneous SFR and the SFR inferred from L_{IR} . Because the galaxies have low initial gas fractions (see L14 for details), the stellar mass increases by a relatively small amount over the course of a simulation; consequently, a given simulation primarily moves up and then down in the SFR- M_* plot as the SFR is increased during the starburst and then quenched.

In most cases, the inferred and actual positions of the simulated galaxies in the SFR- M_* plot agree because the IR-inferred SFR and instantaneous SFR values are similar and the true M_* val-

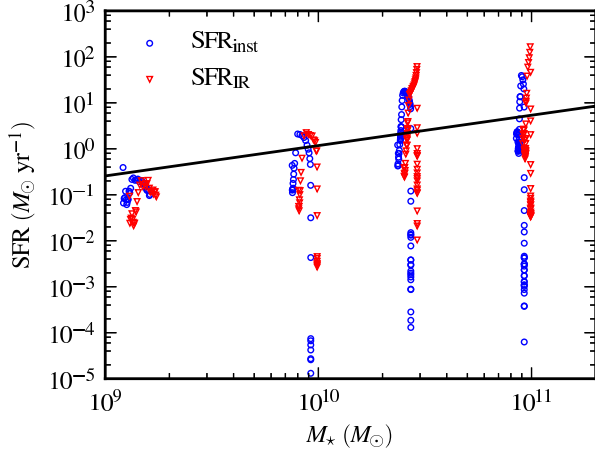


Figure 4. SFR vs. M_* for the major merger simulations. The blue circles indicate that the true instantaneous SFR is used, whereas the red triangles indicate that the SFR value is inferred from L_{IR} . In both cases, the true M_* is used (but for clarity, the M_* values for the red triangles have been increased by 0.03 dex). The solid black line is the best fit to the $z \sim 0.2 - 0.4$ star-forming galaxies of Karim et al. (2011). For the recently quenched galaxies, the inferred and actual locations in the SFR– M_* plane differ significantly (i.e., there are many blue circles that lie significantly below all of the red triangles).

ues are used for both.³ However, for the post-starburst phase of the strong-starburst mergers, this is not the case; instead, the inferred and true locations in the SFR– M_* plot differ significantly (i.e., there are many blue circles that lie significantly below all of the red triangles). Because the IR-inferred SFR overestimates the true SFR in this phase, use of the IR-inferred SFR leads to the conclusion that the recently quenched galaxies are much closer to the SFR– M_* relation of actively star-forming galaxies (the black line in Fig. 4) than they actually are. This effect may also cause the apparent scatter in the SFR– M_* relation to be less than the true scatter (see also Schaerer et al. 2013), but cosmological simulations are necessary to quantify the effect on the scatter, which depends on the abundance of sufficiently strong starbursts and the duration of the overestimate. Unfortunately, even state-of-the-art cosmological simulations are not yet suitable for such an analysis because of their relatively limited resolution (Sparre et al. 2014b).

4 DISCUSSION

4.1 Implications and scope of the overestimation

Because of the SFR overestimation demonstrated above, when one uses L_{IR} to infer the SFR of galaxies that have been recently quenched, inaccurate conclusions are likely. For example, as we have demonstrated, the IR-inferred SFR may suggest that a galaxy lies closer to the SFR– M_* relation than it actually does. Similarly, FIR emission from AGN host galaxies is often considered evidence that AGN do not quench star formation, which would contradict many theoretical models (e.g. Springel et al. 2005a; Hopkins et al.

³ Uncertainties in how the stellar mass is inferred from observations can also have important consequences for the resulting SFR– M_* relation (e.g. Michałowski et al. 2012).

2006). However, the results presented above suggest that if quenching happens rapidly (on timescales of order 100 Myr), as is suggested by simulations, detection of FIR emission from AGN hosts does not (necessarily) imply that star formation is ongoing in those galaxies. Other topics for which this overestimation can have significant implications include the FIR–radio correlation (see Condon 1992 for a review) and the Kennicutt–Schmidt relation.

Because of the typical depths of FIR imaging, the potential bias during the post-starburst phase that we have demonstrated is most serious for observations of low-redshift galaxies and stacking analyses of high-redshift galaxies; i.e., for many post-starburst galaxies, SFR_{IR} may overestimate the instantaneous SFR, but L_{IR} may be less than the detection threshold and thus render the overestimate irrelevant. We stress that for SFR (SSFR) values of as high as $\sim 10 M_{\odot} \text{ yr}^{-1}$ ($\sim 10^{-10} \text{ yr}^{-1}$), the instantaneous SFR can be overestimated by factors of a few or more. This is consistent with the results of Utomo et al. (2014), who presented observational evidence that indicates that the SFRs inferred from a combination of UV and IR luminosities overestimate the true values for the same (S)SFR range as in the simulations. Thus, this overestimation is clearly relevant even for existing observational surveys and will become even more important as detection limits are pushed lower using e.g. ALMA.

Furthermore, it is important to note that the overestimation problem is not limited to the specific situation studied here (low-redshift galaxy mergers); rather, whenever the SFR declines sufficiently rapidly, regardless of the absolute SFR values and the quenching mechanism, this overestimation should occur. Indeed, this overestimation is also present in the post-starburst phase of simulations of $z \sim 2 - 3$ galaxy mergers (see fig. 1 of Hayward et al. 2011).

4.2 Possible solutions

One method to correct IR-inferred SFRs for contamination from older stellar populations is to subtract the diffuse component of the dust emission, which is likely heated predominantly by the diffuse interstellar radiation field and thus connected with older stellar populations rather than recently formed stars (e.g. Smith et al. 1994; Smith & Harvey 1996; Groves et al. 2012; Leroy et al. 2012; Lo Faro et al. 2013). However, such a correction requires spatially resolved, multi-wavelength IR data, which are typically available only for low-redshift galaxies. It is perhaps possible to calibrate corrections using local galaxies and apply them to high-redshift galaxies, but it is unclear that such a technique would be effective because of the significant differences between the properties of low- and high-redshift galaxies.

Another possible approach for avoiding this overestimation is to use SFR tracers other than the IR or a ‘ladder of SFR indicators’ (Wuyts et al. 2011a,b). Radio emission is particularly promising because it is insensitive to dust obscuration and contributions from older stellar populations (Murphy et al. 2011). However, one must be careful to account for other sources of radio emission. Recombination lines are another type of SFR tracer that is insensitive to contamination from older stellar populations. However, the most commonly used recombination line, $\text{H}\alpha$, must be corrected for dust attenuation, and our results suggest that in the post-starburst regime, the effects of dust are particularly nefarious: suppose that the SFR inferred from the IR luminosity is greater than that inferred from the UV emission or recombination lines. The usual interpretation is that dust attenuation causes the UV-optical tracers to underestimate the true SFR; thus, the IR estimate is more accurate. However, the

effect that we have demonstrated works in the opposite direction: dust attenuation of older stars can cause the IR to overestimate the SFR. Consequently, when UV-optical and IR SFR indicators disagree, it is unclear a priori which is closer to the truth.

Because of this degeneracy, it is best to use broadband SED modelling, a multi-wavelength approach that accounts for both unobserved and obscured star formation and that can place meaningful constraints on the star formation history rather than just a single value of the SFR that corresponds to a somewhat ill-defined time-averaged SFR. Multiple potentially suitable tools, including MAGPHYS (da Cunha et al. 2008), CIGALE (Noll et al. 2009; Serra et al. 2011), and CHIBURST (Dopita et al. 2005, 2006a,b; Groves et al. 2008; Martínez-Galarza et al. 2011; R. Martínez-Galarza et al., in preparation), have been developed for this task. Application of one of these tools (MAGPHYS) to simulated SEDs suggests that the inferred SFRs are indeed more accurate than the IR-inferred SFRs (C. Hayward & D. Smith, submitted), which has also been suggested based on observational evidence (Smith et al. 2012; Rowlands et al. 2014; Utomo et al. 2014). The aforementioned tools and similar methods may be able to overcome the shortcomings of simple SFR indicators such as the IR luminosity and thus fully leverage the wealth of multiwavelength data that has become available in recent years.

5 CONCLUSIONS

We have used a set of mock SEDs generated by performing dust radiative transfer on hydrodynamical simulations of isolated disc galaxies and galaxy mergers to investigate the effectiveness of the IR luminosity at recovering the true instantaneous SFR of the simulated galaxies. Our principal conclusions are the following:

(i) For most galaxies (i.e., quiescently star-forming disc galaxies and minor mergers), the SFR inferred from L_{IR} agrees very well with the true SFR.

(ii) In the simulations in which a strong starburst occurs, L_{IR} can significantly overestimate the SFR after the peak of the starburst. The reason for this overestimation is that although the SFR decreases rapidly from the peak, there is still significant IR emission from dust heated by the stars formed during, and even before, the starburst.

(iii) The magnitude of the overestimate is greater for lower SSFR values. However, the instantaneous SSFR value is not the sole determinant of the contribution of older stellar populations to the dust heating because for fixed SSFR, the overestimation is more severe in the post-starburst phase of the simulations. Thus, the time evolution of the SSFR, not just the current value, is an important determinant of how well the IR-inferred SFR traces the true SFR.

(iv) This overestimation may have significant implications for e.g. the SFR-stellar mass relation. In particular, it may cause the number of quenched galaxies and degree to which galaxies are quenched to be underestimated.

The results presented in this work highlight the need for caution when applying simple SFR tracers to galaxies for which the underlying assumptions may not hold. More-sophisticated techniques, such as SED modelling, should be used when possible, but one must also mind the caveats and potential inherent degeneracies in these techniques.

ACKNOWLEDGMENTS

We thank Caitlin Casey, Mattia Fumagalli, Xavier Koenig, Barry Rothberg, Daniel Schaerer, Beverly Smith, Dan Smith, and Tomo Totani for providing useful comments on the manuscript, and we especially thank Samir Salim and the anonymous referee for their very detailed comments, which led to significant improvements to the manuscript. CCH is grateful to the Klaus Tschira Foundation for financial support and acknowledges the hospitality of the Aspen Center for Physics, which is supported by the National Science Foundation Grant No. PHY-1066293. HAS and LL acknowledge partial support from NASA grants NNX12AI55G and NNX10AD68G, and JPL RSA contract 1369566. The simulations in this paper were performed on the Odyssey cluster supported by the FAS Research Computing Group at Harvard University. This research has made use of NASA's Astrophysics Data System.

REFERENCES

- Brinchmann J., Charlot S., White S. D. M., Tremonti C., Kauffmann G., Heckman T., Brinkmann J., 2004, *MNRAS*, 351, 1151
 Calzetti D. et al., 2010, *ApJ*, 714, 1256
 Condon J. J., 1992, *ARA&A*, 30, 575
 Cox T. J., Dutta S. N., Di Matteo T., Hernquist L., Hopkins P. F., Robertson B., Springel V., 2006, *ApJ*, 650, 791
 Cox T. J., Jonsson P., Somerville R. S., Primack J. R., Dekel A., 2008, *MNRAS*, 384, 386
 da Cunha E., Charlot S., Elbaz D., 2008, *MNRAS*, 388, 1595
 Daddi E. et al., 2007, *ApJ*, 670, 156
 Dopita M. A. et al., 2006a, *ApJS*, 167, 177
 Dopita M. A. et al., 2006b, *ApJ*, 647, 244
 Dopita M. A. et al., 2005, *ApJ*, 619, 755
 Elbaz D. et al., 2011, *A&A*, 533, A119
 Fumagalli M. et al., 2013, arXiv:1308.4132
 Groves B., Dopita M. A., Sutherland R. S., Kewley L. J., Fischera J., Leitherer C., Brandl B., van Breugel W., 2008, *ApJS*, 176, 438
 Groves B. et al., 2012, *MNRAS*, 426, 892
 Hayward C. C., Jonsson P., Kereš D., Magnelli B., Hernquist L., Cox T. J., 2012, *MNRAS*, 424, 951
 Hayward C. C., Kereš D., Jonsson P., Narayanan D., Cox T. J., Hernquist L., 2011, *ApJ*, 743, 159
 Hayward C. C., Narayanan D., Kereš D., Jonsson P., Hopkins P. F., Cox T. J., Hernquist L., 2013, *MNRAS*, 428, 2529
 Hayward C. C., Torrey P., Springel V., Hernquist L., Vogelsberger M., 2014, *MNRAS*, 442, 1992
 Hopkins P. F., Hernquist L., Cox T. J., Di Matteo T., Robertson B., Springel V., 2006, *ApJS*, 163, 1
 James A., Dunne L., Eales S., Edmunds M. G., 2002, *MNRAS*, 335, 753
 Jonsson P., 2006, *MNRAS*, 372, 2
 Jonsson P., Cox T. J., Primack J. R., Somerville R. S., 2006, *ApJ*, 637, 255
 Jonsson P., Groves B. A., Cox T. J., 2010, *MNRAS*, 403, 17
 Kelson D. D., Holden B. P., 2010, *ApJL*, 713, L28
 Kennicutt R. C., 1998a, *ApJ*, 498, 541
 Kennicutt R. C., 1998b, *ARA&A*, 36, 189
 Kennicutt R. C. et al., 2007, *ApJ*, 671, 333
 Kennicutt R. C., Evans N. J., 2012, *ARA&A*, 50, 531
 Kennicutt, Jr. R. C. et al., 2009, *ApJ*, 703, 1672
 Kroupa P., 2001, *MNRAS*, 322, 231
 Lanz L., Hayward C. C., Zezas A., Smith H. A., Ashby M. L. N., Brasington N., Fazio G. G., Hernquist L., 2014, *ApJ*, 785, 39 (L14)
 Lanz L. et al., 2013, *ApJ*, 768, 90
 Lee N. et al., 2013, *ApJ*, 778, 131
 Leitherer C. et al., 1999, *ApJS*, 123, 3
 Leroy A. K. et al., 2012, *AJ*, 144, 3
 Lo Faro B. et al., 2013, *ApJ*, 762, 108
 Magnelli B. et al., 2012, *A&A*, 539, A155

- Martínez-Galarza J. R., Groves B., Brandl B., de Messieres G. E., Indebetouw R., Dopita M. A., 2011, *ApJ*, 738, 176
- Michałowski M. J., Dunlop J. S., Cirasuolo M., Hjorth J., Hayward C. C., Watson D., 2012, *A&A*, 541, A85
- Murphy E. J. et al., 2011, *ApJ*, 737, 67
- Narayanan D., Cox T. J., Hayward C. C., Younger J. D., Hernquist L., 2009, *MNRAS*, 400, 1919
- Narayanan D., Davé R., 2012, *MNRAS*, 423, 3601
- Narayanan D. et al., 2010a, *MNRAS*, 407, 1701
- Narayanan D., Hayward C. C., Cox T. J., Hernquist L., Jonsson P., Younger J. D., Groves B., 2010b, *MNRAS*, 401, 1613
- Noeske K. G. et al., 2007, *ApJL*, 660, L43
- Noll S., Burgarella D., Giovannoli E., Buat V., Marcillac D., Muñoz-Mateos J. C., 2009, *A&A*, 507, 1793
- Reddy N. A., Pettini M., Steidel C. C., Shapley A. E., Erb D. K., Law D. R., 2012, *ApJ*, 754, 25
- Relaño M., Kennicutt, Jr. R. C., 2009, *ApJ*, 699, 1125
- Rodighiero G. et al., 2010, *A&A*, 518, L25
- Rosario D. J. et al., 2012, *A&A*, 545, A45
- Rosario D. J. et al., 2013, *A&A*, 560, A72
- Rowlands K. et al., 2014, *MNRAS*, 441, 1017
- Salim S. et al., 2005, *ApJL*, 619, L39
- Salim S. et al., 2009, *ApJ*, 700, 161
- Sauvage M., Thuan T. X., 1992, *ApJL*, 396, L69
- Schaerer D., de Barros S., Sklias P., 2013, *A&A*, 549, A4
- Schiminovich D. et al., 2007, *ApJS*, 173, 315
- Schmidt M., 1959, *ApJ*, 129, 243
- Serra P., Amblard A., Temi P., Burgarella D., Giovannoli E., Buat V., Noll S., Im S., 2011, *ApJ*, 740, 22
- Sklias P. et al., 2014, *A&A*, 561, A149
- Smith B. J., Harvey P. M., 1996, *ApJ*, 468, 139
- Smith B. J., Harvey P. M., Colome C., Zhang C. Y., Difrancesco J., Pogge R. W., 1994, *ApJ*, 425, 91
- Smith D. J. B. et al., 2012, *MNRAS*, 427, 703
- Snyder G. F., Cox T. J., Hayward C. C., Hernquist L., Jonsson P., 2011, *ApJ*, 741, 77
- Snyder G. F., Hayward C. C., Sajina A., Jonsson P., Cox T. J., Hernquist L., Hopkins P. F., Yan L., 2013, *ApJ*, 768, 168
- Sparre M. et al., 2014a, *ApJ*, 785, 150
- Sparre M. et al., 2014b, arXiv:1409.0009
- Springel V., 2005, *MNRAS*, 364, 1105
- Springel V., Di Matteo T., Hernquist L., 2005a, *ApJ*, 620, L79
- Springel V., Di Matteo T., Hernquist L., 2005b, *MNRAS*, 361, 776
- Springel V., Hernquist L., 2003, *MNRAS*, 339, 289
- Totani T., Takeuchi T. T., Nagashima M., Kobayashi M. A. R., Makiya R., 2011, *PASJ*, 63, 1181
- Utomo D., Kriek M., Labbé I., Conroy C., Fumagalli M., 2014, *ApJL*, 783, L30
- Walterbos R. A. M., Greenawalt B., 1996, *ApJ*, 460, 696
- Wuyts S., Cox T. J., Hayward C. C., Franx M., Hernquist L., Hopkins P. F., Jonsson P., van Dokkum P. G., 2010, *ApJ*, 722, 1666
- Wuyts S. et al., 2011a, *ApJ*, 738, 106
- Wuyts S. et al., 2011b, *ApJ*, 742, 96